

Nonmagnetic doping induced quantum anomalous Hall effect in topological insulators

Shifei Qi,^{1,2} Ruiling Gao,^{3,1} Maozhi Chang,^{3,1} Tao Hou,² Yulei Han,^{2,*} and Zhenhua Qiao^{1b,2,†}

¹Department of Physics, Hebei Normal University, Shijiazhuang, Hebei 050024, China

²ICQD, Hefei National Laboratory for Physical Sciences at Microscale, CAS Key Laboratory of Strongly-Coupled Quantum Matter Physics, and Department of Physics, University of Science and Technology of China, Hefei, Anhui 230026, China

³Institute of Materials Science, Shanxi Normal University, Linfen, Shanxi 041004, China



(Received 10 July 2019; revised 20 June 2020; accepted 27 July 2020; published 17 August 2020)

Quantum anomalous Hall effect (QAHE) has been experimentally observed in magnetically doped topological insulators. However, ultralow temperatures (usually below 300 mK), which are mainly attributed to inhomogeneous magnetic doping, become a daunting challenge for potential applications. Here, a *nonmagnetic*-doping strategy is proposed to produce ferromagnetism and realize QAHE in topological insulators. We numerically demonstrate that magnetic moments can be induced by nonmagnetic nitrogen or carbon substitution in Bi₂Se₃, Bi₂Te₃, and Sb₂Te₃, while only nitrogen-doped Sb₂Te₃ system can exhibit long-range ferromagnetism and preserve large bulk band gaps. We further show that its corresponding thin film can harbor QAHE at temperatures of 17–29 Kelvin, which is two orders of magnitude higher than typical realized temperatures in similar systems. Our proposed *nonmagnetic* doping scheme may shed light on experimental realization of high-temperature QAHE in topological insulators.

DOI: [10.1103/PhysRevB.102.085419](https://doi.org/10.1103/PhysRevB.102.085419)

I. INTRODUCTION

Quantum anomalous Hall effect (QAHE) [1] is the counterpart of quantum Hall effect in the absence of strong magnetic field. Due to topological protection from the spatial separation, the chiral edge modes of QAHE have immense application potential in future dissipationless quantum devices [2]. Since its initial predication in a honeycomb-lattice model [1], numerous efforts have been made to explore platforms for realizing QAHE in related material systems [3–14]. The virtue of inherent strong spin-orbit coupling in \mathbb{Z}_2 topological insulators (TIs) [15,16] has narrowed the search for suitable materials possessing intrinsic magnetism. One possible way to induce magnetism in TIs is to dope magnetic elements [6,17–20]. This approach has led to the first experimental realization of QAHE in Cr/V-doped (Bi,Sb)₂Te₃ thin films [21–24]. So far, all experimentally observed QAHEs in doped TIs were achieved at extremely low temperatures, typically ~30 mK, making drastically increasing the QAHE observation temperature a challenge for realistic applications.

In magnetically doped (Bi,Sb)₂Te₃ thin films, inhomogeneous ferromagnetism is considered to be one of the main factors that lead to the unexpected low QAHE observation temperature [25]. Another possible factor is the appearance of the dissipative conduction channels due to metallization of the magnetically doped TIs bulklike region [26]. Empirically, codoping is an effective way to improve ferromagnetic order, as confirmed in dilute magnetic semiconductors (DMSs) [17]. Our theoretical study showed that the observed

temperature of QAHE can increase by codoping Sb₂Te₃ with *p*-type vanadium and *n*-type iodine dopants [27]. Indeed, an increased QAHE temperature was observed in Cr- and V-codoped (Bi,Sb)₂Te₃ thin films [28]. At the optimal Cr/V ratio, full quantization was achieved at 300 mK, an order of magnitude higher than that with single dopants. The obtained Hall hysteresis loop is more squarelike, suggesting a reduced magnetic inhomogeneity in Cr- and V-codoped (Bi,Sb)₂Te₃ thin films [28]. In the study of DMSs, researchers showed that homogeneous DMS systems by magnetic doping is unrealistic [17]. By careful tuning of crystal growth conditions or utilizing a codoping method, magnetic inhomogeneity can only be suppressed more or less. This is because strong attractive interaction from doped magnetic impurities are difficult to suppress their aggregation in DMSs [29].

Alternatively, many materials with nonmagnetic dopants exhibited robust high-temperature ferromagnetism. For example, carbon-doped ZnO films showed ferromagnetism with Curie temperature higher than 400 K [30,31]. Above room temperature, ferromagnetism was also observed in carbon-doped hexagonal boron nitride [32]. Doping nonmagnetic fluorine in two-dimensional antimonene also reaches robust above-room-temperature ferromagnetism [33]. More importantly, no strong attractive interaction exists between nonmagnetic dopants, naturally avoiding the formation of inhomogeneous ferromagnetism and dissipative conduction channels. Therefore, it is of great interest to explore the possibility of realizing high-temperature QAHE in nonmagnetically doped TIs.

In this paper, we showed that high-temperature QAHE can be realized in nonmagnetically doped TIs, e.g., by doping nonmagnetic C or N atoms in Sb₂Te₃ TI thin films. We took three representative TIs (i.e., Bi₂Se₃, Bi₂Te₃, and Sb₂Te₃)

*Corresponding author: hanyulei@ustc.edu.cn

†Corresponding author: qiao@ustc.edu.cn

as examples, and found that their magnetic moments can be induced via nonmagnetic C or N substitution. For all doping concentrations considered, only the N-doped Sb_2Te_3 system exhibits long-range ferromagnetic order. Moreover, an estimated Curie temperature of 17–29 Kelvin can be reached at the concentration of 11–22% N-doped Sb_2Te_3 . Aside from the bulk properties, the band gaps of the corresponding thin films can also be as large as 17 meV, large enough to sustain ferromagnetic order at the high Curie temperature. Explicit Berry curvature calculations further confirm that the N-doped Sb_2Te_3 thin films can harbor QAHE. Our proposed nonmagnetic doping approach offers a versatile route to realize QAHE in TIs and related materials.

II. COMPUTATIONAL METHODS

Our first-principles calculations were performed using the projected augmented-wave method [34] as implemented in the VIENNA AB INITIO SIMULATION PACKAGE [35]. The generalized gradient approximation of the Perdew-Burke-Ernzerhof type was used to treat the exchange-correlation interaction [36]. Our nonmagnetic doping in TIs is that all atoms in a layer of TIs are substituted, which is similar to that in MnBi_2Te_4 where all Mn in an atom layer and no random Mn distribute. $1 \times 1 \times 1$ Bi_2Se_3 , Bi_2Te_3 , and Sb_2Te_3 cells were chosen in this study. For thin-film calculations, the film thickness was chosen to be five quintuple layers (QLs). A vacuum buffer space of 30 Å was used to prevent coupling between adjacent slabs. The kinetic energy cutoff was set to 400 eV. During structural relaxation, all atoms were allowed to relax until the Hellmann-Feynman force on each atom was less than 0.01 eV/Å. The Brillouin-zone integration was carried out by using $15 \times 15 \times 2$ and $9 \times 9 \times 1$ Monkhorst-Pack grids for bulk and thin-film systems, respectively. Unless mentioned otherwise, spin-orbit coupling was considered in all calculations. The Curie temperature T_C was estimated within the mean-field approximation $k_B T_C = \frac{2}{3} x J$ [37], where k_B is the Boltzmann constant, x is the doping concentration, and J is the exchange parameter obtained from the total energy difference between ferromagnetic and antiferromagnetic configurations at different doping concentrations.

III. FORMATION ENERGY

Let us first discuss the possibility of doping nonmagnetic N and C atoms in Bi_2Se_3 , Bi_2Te_3 , and Sb_2Te_3 TIs. As a concrete example, the bulk structure of Sb_2Te_3 is shown in Fig. 1(a). Each QL [Fig. 1(a)] consists of two equivalent Te atoms (Te_1), two equivalent Sb atoms, and a third Te atom (Te_2). Atoms within one QL are coupled by a strong chemical bond, whereas weak van der Waals forces hold QLs together. We placed the impurities at Se or Te site in $2 \times 2 \times 1$ bulk Bi_2Se_3 , Bi_2Te_3 , and Sb_2Te_3 TIs, and compare their formation energies, which can be computed using the following expression:

$$\Delta H_F = E_{\text{tot}}^{\text{DB}} - E_{\text{tot}}^{\text{B}} - \sum n_i \mu_i, \quad (1)$$

where $E_{\text{tot}}^{\text{DB}}$ is the total energy of the supercell including one nonmagnetic impurity, $E_{\text{tot}}^{\text{B}}$ is the total energy of the supercell, μ_i is the chemical potential for the species i (host

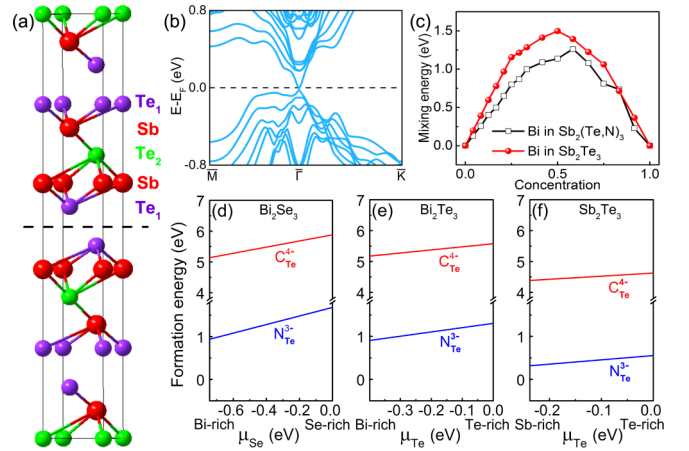


FIG. 1. (a) Structure illustration of bulk Sb_2Te_3 . (b) Band structure of Sb_2Te_3 with five QLs. (c) Mixing energy of Bi in the $\text{Sb}_2(\text{Te},\text{N})_3$ and Sb_2Te_3 systems. Formation energies of the most stable configurations of single C- or N-doped Bi_2Se_3 (d), Bi_2Te_3 (e), and Sb_2Te_3 (f) as a function of the host element chemical potentials, respectively.

atoms or dopants), and n_i is the corresponding number that has been added to or removed from the supercell. We chose rhombohedral Bi, rhombohedral Sb, hexagonal Se, hexagonal Te, nonmagnetic body centered-cubic (bcc) C, and antiferromagnetic hexagonal N as a reference to evaluate the chemical potentials of the elements. Detailed computational methods can be found in Ref. [38].

As displayed in Figs. 1(d)–1(f), the calculated formation energies indicate that Se or Te substitutional sites are preferred by the nonmagnetic N atoms, because N possesses less formation energies (about 1.0 eV) in the whole range of the accessible host element chemical potentials. Particularly for Sb_2Te_3 , the formation energy of N substitution is only in the range of 0.25–0.50 eV for the whole host element chemical potentials. It seems that the estimated formation energy of C substituted Se or Te is much larger than that of N substituted Se or Te, which is about 5.0 eV. While it is noteworthy that C-doped ZnO can also be realized in experiments even if the estimated formation energy of C substituted O in ZnO is about 5.3 eV [30]. Therefore, one can reasonably conclude that N- or C-substituted Bi_2Se_3 , Bi_2Te_3 , and Sb_2Te_3 TIs can be experimentally produced.

IV. MAGNETIC PROPERTIES

Next, we focused on whether such nonmagnetic dopants in TIs can induce magnetic moments, and further establish the long-range ferromagnetism, as that confirmed in C-doped ZnO [30,31]. Table I includes the magnetic moments of C- and N-substituted Bi_2Se_3 , Bi_2Te_3 , and Sb_2Te_3 TIs were included. For the C-doped systems, our results show that magnetic moments can always arise when C substitutes at Te_1 or Se_1 site. The corresponding total moments are, respectively, 0.38, 0.56, and 0.10 μ_B for the three different TI systems. While for the C-doped Bi_2Te_3 , the total moment of 1.64 μ_B can be induced in the case of C substitution at Te_2 site. Compared with the C-doping, magnetic moments can always be induced

TABLE I. Total magnetic moments (M_{tot}) and magnetic moments contributed by C (M_C) or N (M_N) atom in C- or N-doped bulk Bi_2Se_3 , Bi_2Te_3 , and Sb_2Te_3 . X represents Se or Te atom. The unit of magnetic moment is μ_B .

TIs	C-doped TIs				N-doped TIs			
	X_1		X_2		X_1		X_2	
	M_C	M_{tot}	M_C	M_{tot}	M_N	M_{tot}	M_N	M_{tot}
Bi_2Se_3	0.19	0.38	0.00	0.00	0.62	1.00	0.30	0.97
Bi_2Te_3	0.24	0.56	0.38	1.64	0.56	1.00	0.18	0.69
Sb_2Te_3	0.06	0.13	0.00	0.00	0.00	0.00	0.14	0.58

by the N dopant except in the case of N substitution at the Te_1 site of Sb_2Te_3 .

The magnetic moments in N- and C-doped TIs can be understood from the calculated local density of states (LDOS) [see N-doped Sb_2Te_3 in Fig. 2(a)]. Strong coupling between the $2p$ -orbital of N and Te $5p$, Sb $5s/5p$ orbitals results in the above orbitals near the Fermi level to split along spin directions. The spin-up bands are nearly fully occupied while the spin-down bands are partially filled, leading to a magnetic moment of $0.58 \mu_B$ per unit cell. The spin-density distribution in Fig. 2(b) further reveals that the ferromagnetism arises from a synergistic effect of the N-dopant and its first- and second-nearest-neighboring Sb and Te atoms in one QL. The neighboring Sb and Te atoms are ferromagnetically coupled to the N atom. No d state is observed at the Fermi level, confirming the pure sp-electron ferromagnetism. In addition, little amount of spin polarization along the other direction is observed. Thus, one can say that the whole QL can be spin polarized (long-range ferromagnetism) by substituting only one Te atom with one N atom in Sb_2Te_3 . In fact, the magnetic ground states for N-doped Sb_2Te_3 have been calculated with the inclusion of spin-orbit coupling, and the

results indicate that out-of-plane spin polarization is slightly preferred.

One can also find that no local magnetic moment is induced for N-substitution at the Te_1 site of Sb_2Te_3 . As shown in Fig. 2(d), it can be attributed to the strong bonding interaction existing between the substituted N atom and the nearest Sb atom, which decreases the interaction of this Sb atom and its surrounding Te (Te_2 site) atoms in the same QL while, in the case of N-substitution at Te_2 site, the bonding interaction between the substituted N atom and its nearest Sb atom is weaker than that in the case of N substitution at Te_1 . From Fig. 2(c), one can see that this weaker bonding interaction does not decrease the interaction between the substituted N atom and its surrounding Sb atoms, which agrees with the observation in Fig. 2(a).

V. BAND STRUCTURES AND QUANTUM ANOMALOUS HALL EFFECT

Aside from the ferromagnetic ordering of N- and C-doped TIs, two other prerequisites [2] for the observation of QAHE include (1) the bulk gap exists in N- and C-doped TIs and (2) the surface band gap can be opened due to the ferromagnetic exchange field. To this point, let us continue to investigate the variance of band structures due to the C- and N-doping. First, we focused on the bulk band structures of N- or C-doped Bi_2Se_3 , Bi_2Te_3 , and Sb_2Te_3 TIs. Figure 3(a) displays the bulk band structure of 11% N-doped Sb_2Te_3 at the Te_2 site, opening a small bulk gap about 9 meV. In fact, the bulk gap of N-doped Sb_2Te_3 can be dramatically increased to 39 meV [see Fig. 3(b)] when N-doping concentration increases from 11% to 22%. In 11% N-doped Sb_2Te_3 , further analysis of the characters of different elements [see Figs. 3(a1)–3(a3)] reveals that the valence band (conduction band) close to the band gap is dominated by Te (Sb) atoms, while N contributes mainly to the lower part of the valence bands. These results directly reflect the strong bonding interaction between N and surrounding Sb atoms due to the larger electronegativity of N. If doping concentration is increased to 22%, the contribution from Sb (Te) atoms to conduction (valence band) band close to the gap obviously decreases [see Figs. 3(b1)–3(b3)]. This is because more N dopants substitute Te atoms, then more strong bonding interaction between N and the surrounding Sb atoms arises, and the resulting large energy difference between the bonding and antibonding orbitals helps to enlarge the bulk gap. In addition, our results presented in Figs. 3(c)–3(f) confirm that appropriate in-plane tensile strains cannot only greatly enlarge the bulk gap from 9 meV to 46 (1% tensile strain), 74 meV (2% tensile strain), and 85 meV (3% tensile strain), but also shift the Fermi level closer to the bulk band gap for the 11% N-doped Sb_2Te_3 . The strain effect on bulk band gap and Fermi level will be beneficial for realization of high-temperature QAHE in N-doped Sb_2Te_3 . Calculated results for other doping configurations can be found in the Supplemental Material. Unfortunately, no global bulk band gap appears in these systems (see Supplemental Material [39]). Thus, our results prove that N-doped Sb_2Te_3 is an ideal candidate for high-temperature QAHE and its corresponding bulk gap can be modulated via doping concentration or applying in-plane strain.

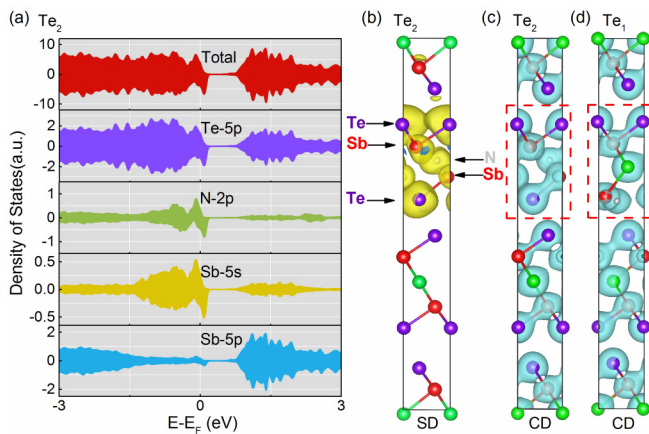


FIG. 2. (a) Total and projected density of states for Sb $5p$, Te $5p$, and N $2p$ orbitals in N-doped Sb_2Te_3 . (b) Spin density (SD) distribution in N-doped Sb_2Te_3 at Te_2 site. Yellow and blue isosurfaces correspond to the majority and minority spin density, respectively. (c), (d) Charge density (CD) distribution in N-doped Sb_2Te_3 at Te_2 (c) and Te_1 (d) sites, respectively.

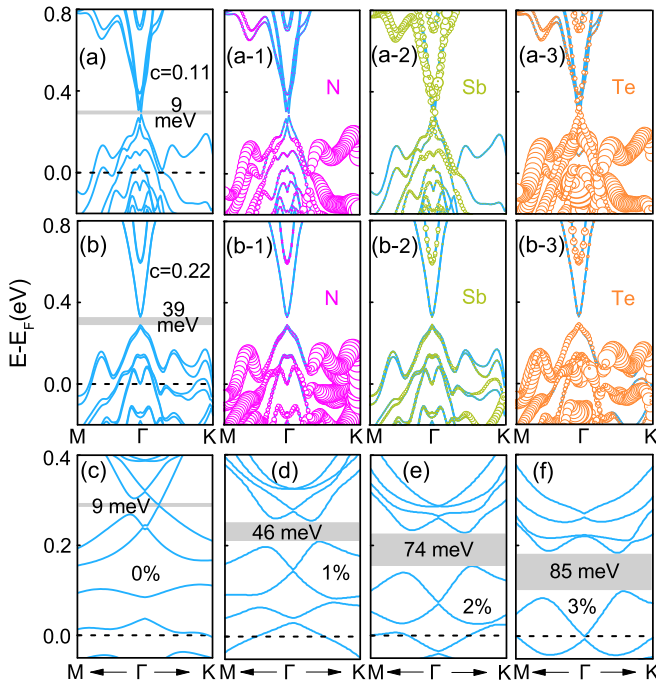


FIG. 3. Band structures of N-doped Sb_2Te_3 . (a) At 11% N-doping concentration, the bulk gap is about 9 meV; (a1)–(a3) Different characters of the bands shown in panel (a), obtained by projecting the Kohn-Sham states onto the local orbitals of a single atom for each element. (b) At 22% N-doping concentration, the bulk gap enlarges to 39 meV. (b1)–(b3) Different characters of the bands shown in panel (b). (c) Zoom-in of N-doped Sb_2Te_3 band structure around the band gap. (d)–(f) Band structures of N-doped Sb_2Te_3 under different in-plane tensile strains. Dashed line denotes the Fermi level.

So far, the above results strongly suggest that N-doped Sb_2Te_3 is a highly desirable candidate for designing high-temperature QAHE. In principle, one still needs to see whether its corresponding thin-film system can also open sizable band gaps or not. From analyzing the band structures, we showed that these thin-film systems can indeed harbor topological states (i.e., QAHE) at different doping concentrations. In the absence of dopants, the thin film of 5QLs Sb_2Te_3 hosts a massless Dirac fermion, manifested as the hallmark linear Dirac dispersion near the gamma point [40] [see Fig. 1(c)]. When N dopants are introduced, the Dirac fermion acquires a finite mass to open up a surface band gap, due to the presence of induced ferromagnetism. This satisfies the prerequisites to form QAHEs [16].

Figure 4 displays the band structures and Berry curvatures along the high-symmetry line near the Γ point at two different N-doping concentrations of 7% [(a), (b)] and 13% [(c), (d)], respectively. One can find that the band gap increases along with the doping concentration. It is noteworthy that our calculated band structure for 7% doping without spin opens a small gap about 7 meV due to the intersurface hybridization. When the spin degree of freedom is invoked, the strong ferromagnetic exchange field closes the band gap and forms band crossings between spin-up and -down bands, which then

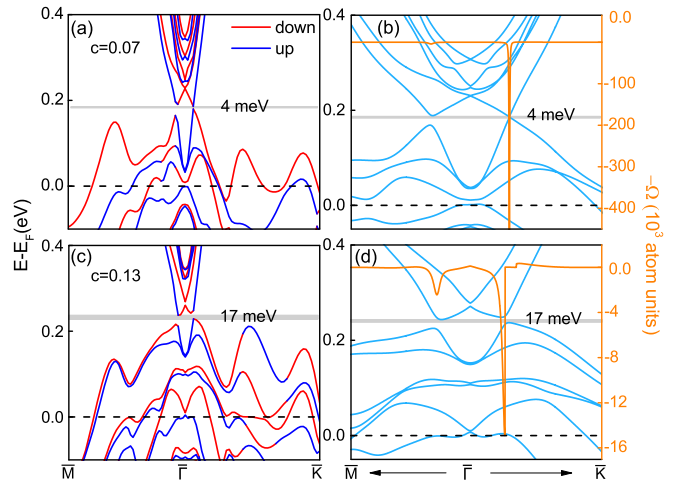


FIG. 4. Band structures of N doped Sb_2Te_3 thin film with a thickness of five QLs at 7% (a), (b) and 13% (c), (d) N-doping concentrations, respectively. Spin-up and -down bands are, respectively, highlighted in red and blue. (a), (c) Band structures with spins. (b), (d) Zoom-in of the band structures near the Γ point in panels (a) and (c) and corresponding Berry curvatures.

naturally open up topologically nontrivial band gap when the spin-orbit coupling is considered.

Quantitatively, one can provide unambiguous evidence for the manifestation of QAHEs by integrating the Berry curvature of the occupied valence [41,42]. Figures 4(b) and 4(d) display the Berry curvature distribution along high symmetry lines, which exhibits a large negative peak near the Γ point and zero elsewhere. As a consequence, the total integration of the Berry curvatures (i.e., the Hall conductance) must be nonzero. On the other hand, the region with finite Berry curvatures broadens with the increase of the surface band gap, and the curvature peak gradually decreases, implicating the unchanged quantized Hall conductance. Therefore, we showed that the N-doped Sb_2Te_3 thin film can realize the QAHE.

Now, let us estimate the possible QAHE observation temperature. For particular doping concentrations, the Curie temperatures are, respectively, $T_C = 17(29)$ Kelvin at 11% (22%) N-doping concentrations, by using the magnetic coupling strengths (the energy differences between FM and AFM states are, respectively, 10.15 and 14.06 meV for the 11% and 22% N-doped Sb_2Te_3) extracted from our first-principles calculations and the mean-field theory [37]. This indicates that the Curie temperature might be raised along with the doping concentration. But one has to note that higher doping concentrations may decrease the spin-orbit coupling of the whole system.

One merit of N-doping in TIs is that a *nonmagnetic* doping scheme will not result in inhomogeneous distribution that occurs in magnetic dopants. Another one is that dissipative conduction channels due to metallization in magnetic-element-doped TIs cannot be formed by *nonmagnetic* and nonmetal N doping. In our recent study of origin of inhomogeneous ferromagnetism in magnetic-doped TIs, we find that inhomogeneous mixing Bi and Sb in experimental QAHE $(\text{Bi,Sb})_2\text{Te}_3$ systems is the origin of inhomogeneous ferromagnetism [43]. As shown in the Fig. 1(c), we also simulate the effect of

nonmagnetic N doping on the Bi distribution in $(\text{Bi,Sb})_2\text{Te}_3$ system. Compared with the situation of $(\text{Bi,Sb})_2\text{Te}_3$ systems, the mixing energy of Bi in N-doped $(\text{Bi,Sb})_2\text{Te}_3$ systems is lower than that in $(\text{Bi,Sb})_2\text{Te}_3$ systems. It indicates that nonmagnetic N doping can also enhance the inhomogeneity of $(\text{Bi,Sb})_2\text{Te}_3$ system. In addition, there were many materials by nonmagnetic dopants exhibiting robust high-temperature ferromagnetism [30–33]; our work will provide a highly desirable scheme to overcome the difficulty of observing QAHE at high temperatures [21–24].

VI. SUMMARY

In conclusion, our findings demonstrate that nonmagnetic nitrogen-doped TIs provide a versatile route to realize high-temperature QAHE. Our proof-of-principle demonstrations revealed that nonmagnetic N doping results in the formation of bulk gaps, long-range ferromagnetism with moderate Curie

temperatures, and nonzero Berry curvatures. The estimated QAHE observation temperature is 17–29 K in 11–22% N-doped Sb_2Te_3 thin films, which is about two orders of magnitude higher than what was previously reported. By further increasing and tailoring the doping and TI environments, it is feasible to further increase the observation temperature of the QAHE.

ACKNOWLEDGMENTS

This work was financially supported by the NNSFC (No. 11974098 and No. 11974327), Natural Science Foundation of Hebei Province (A2019205037), and Science Foundation of Hebei Normal University (2019B08), Fundamental Research Funds for the Central Universities, Anhui Initiative in Quantum Information Technologies. The Supercomputing services of AM-HPC and USTC are gratefully acknowledged.

-
- [1] F. D. M. Haldane, *Phys. Rev. Lett.* **61**, 2015 (1988).
- [2] K. He, Y. Wang, and Q.-K. Xue, *Annu. Rev. Condens. Matter Phys.* **9**, 329 (2018).
- [3] M. Onoda and N. Nagaosa, *Phys. Rev. Lett.* **90**, 206601 (2003).
- [4] C. X. Liu, X. L. Qi, X. Dai, Z. Fang, and S. C. Zhang, *Phys. Rev. Lett.* **101**, 146802 (2008).
- [5] C. Wu, *Phys. Rev. Lett.* **101**, 186807 (2008).
- [6] R. Yu, W. Zhang, H. J. Zhang, S. C. Zhang, X. Dai, and Z. Fang, *Science* **329**, 61 (2010).
- [7] Z. H. Qiao, S. A. Yang, W. X. Feng, W.-K. Tse, J. Ding, Y. G. Yao, J. Wang, and Q. Niu, *Phys. Rev. B* **82**, 161414(R) (2010).
- [8] Z. F. Wang, Z. Liu, and F. Liu, *Phys. Rev. Lett.* **110**, 196801 (2013).
- [9] K. F. Garrity and D. Vanderbilt, *Phys. Rev. Lett.* **110**, 116802 (2013).
- [10] J. Hu, Z. Zhu, and R. Wu, *Nano Lett.* **15**, 2074 (2015).
- [11] C. Fang, M. J. Gilbert, and B. A. Bernevig, *Phys. Rev. Lett.* **112**, 046801 (2014).
- [12] J. Wang, B. Lian, H. Zhang, Y. Xu, and S. C. Zhang, *Phys. Rev. Lett.* **111**, 136801 (2013).
- [13] G. F. Zhang, Y. Li, and C. Wu, *Phys. Rev. B* **90**, 075114 (2014).
- [14] H. Z. Lu, A. Zhao, and S. Q. Shen, *Phys. Rev. Lett.* **111**, 146802 (2013).
- [15] M. Z. Hasan and C. L. Kane, *Rev. Mod. Phys.* **82**, 3045 (2010).
- [16] X. L. Qi and S. C. Zhang, *Rev. Mod. Phys.* **83**, 1057 (2011).
- [17] T. Jungwirth, J. Sinova, J. Mašek, J. Kučera, and A. H. MacDonald, *Rev. Mod. Phys.* **78**, 809 (2006).
- [18] Y. S. Hor, P. Roushan, H. Beidenkopf, J. Seo, D. Qu, J. G. Checkelsky, L. A. Wray, D. Hsieh, Y. Xia, S. Y. Xu, D. Qian, M. Z. Hasan, N. P. Ong, A. Yazdani, and R. J. Cava, *Phys. Rev. B* **81**, 195203 (2010).
- [19] C. Niu, Y. Dai, M. Guo, W. Wei, Y. Ma, and B. Huang, *Appl. Phys. Lett.* **98**, 252502 (2011).
- [20] P. P. J. Haazen, J. B. Laloe, T. J. Nummy, H. J. M. Swagten, P. Jarillo-Herrero, D. Heiman, and J. S. Moodera, *Appl. Phys. Lett.* **100**, 082404 (2012).
- [21] C.-Z. Chang, J. S. Zhang, X. Feng, J. Shen, Z. C. Zhang, M. Guo, K. Li, Y. Ou, P. Wei, L.-L. Wang, Z.-Q. Ji, Y. Feng, S. H. Ji, X. Chen, J. F. Jia, X. Dai, Z. Fang, S.-C. Zhang, K. He, Y. Y. Wang, L. Lu, X.-C. Ma, and Q.-K. Xue, *Science* **340**, 167 (2013).
- [22] J. G. Checkelsky, R. Yoshimi, A. Tsukazaki, K. S. Takahashi, Y. Kozuka, J. Falson, M. Kawasaki, and Y. Tokura, *Nat. Phys.* **10**, 731 (2014).
- [23] X. Kou, S.-T. Guo, Y. Fan, L. Pan, M. Lang, Y. Jiang, Q. Shao, T. Nie, K. Murata, J. Tang, Y. Wang, L. He, T.-K. Lee, W.-L. Lee, and K. L. Wang, *Phys. Rev. Lett.* **113**, 137201 (2014).
- [24] C. Z. Chang, W. Zhao, D. Y. Kim, H. Zhang, B. A. Assaf, D. Heiman, S.-C. Zhang, C. Liu, M. H. W. Chan, and J. S. Moodera, *Nat. Mater.* **14**, 473 (2015).
- [25] I. Lee, C. K. Kima, J. Leea, S. J. L. Billingea, R. Zhong, J. A. Schneeloch, T. Liua, T. Valla, J. M. Tranquada, G. Gua, and J. C. Seamus Davis, *PNAS* **112**, 1316 (2015).
- [26] M. Mogi, R. Yoshimi, A. Tsukazaki, K. Yasuda, Y. Kozuka, K. S. Takahashi, and Y. Tokura, *Appl. Phys. Lett.* **107**, 182401 (2015).
- [27] S. Qi, Z. Qiao, X. Deng, E. D. Cubuk, H. Chen, W. Zhu, E. Kaxiras, S. B. Zhang, X. Xu, and Z. Zhang, *Phys. Rev. Lett.* **117**, 056804 (2016).
- [28] Y. Ou, C. Liu, G. Y. Jiang, Y. Feng, D. Y. Zhao, W. X. Wu, X. X. Wang, W. Li, C. L. Song, L. L. Wang, W. B. Wang, W. D. Wu, Y. Y. Wang, K. He, X. C. Ma, and Q. K. Xue, *Adv. Mater.* **30**, 1703062 (2018).
- [29] T. Dietl and H. Ohno, *Rev. Mod. Phys.* **86**, 187 (2014).
- [30] H. Pan, J. B. Yi, L. Shen, R. Q. Wu, J. H. Yang, J. Y. Lin, Y. P. Feng, J. Ding, L. H. Van, and J. H. Yin, *Phys. Rev. Lett.* **99**, 127201 (2007).
- [31] S. Zhou, Q. Xu, K. Potzger, G. Talut, R. Grotzschel, J. Fassbender, M. Vinnichenko, J. Grenzer, M. Helm, H. Hochmuth, M. Lorenz, M. Grundmann, and H. Schmidt, *Appl. Phys. Lett.* **93**, 232507 (2008).
- [32] C. Zhao, Z. Xu, H. Wang, J. Wei, W. Wang, X. Bai, and E. Wang, *Adv. Funct. Mater.* **24**, 5985 (2014).

- [33] X. Tang, L. Hu, T. Fan, L. Zhang, L. Zhu, H. Li, H. Liu, J. Liang, K. Wang, Z. Li, S. Ruan, Y. Zhang, D. Fan, W. Chen, Y.-J. Zeng, and H. Zhang, *Adv. Funct. Mater.* **29**, 1808746 (2019).
- [34] P. E. Blöchl, *Phys. Rev. B* **50**, 17953 (1994).
- [35] G. Kresse and J. Furthmüller, *Phys. Rev. B* **54**, 11169 (1996).
- [36] J. P. Perdew, J. A. Chevary, S. H. Vosko, K. A. Jackson, M. R. Pederson, D. J. Singh, and C. Fiolhais, *Phys. Rev. B* **46**, 6671 (1992).
- [37] L. Bergqvist, O. Eriksson, J. Kudrnovsky, V. Drchal, A. Bergman, L. Nordstrom, and I. Turek, *Phys. Rev. B* **72**, 195210 (2005).
- [38] J. M. Zhang, W. G. Zhu, Y. Zhang, D. Xiao, and Y. G. Yao, *Phys. Rev. Lett.* **109**, 266405 (2012).
- [39] See Supplemental Material at <http://link.aps.org/supplemental/10.1103/PhysRevB.102.085419> for the other bulk band structures of N- and C-doped TIs with local magnetic moments including N-doped Bi₂Se₃, N-doped Bi₂Te₃, C-doped Bi₂Se₃, C-doped Bi₂Te₃, and C-doped Sb₂Te₃.
- [40] D. Kong, Y. Chen, J. J. Cha, Q. Zhang, J. G. Analytis, K. Lai, Z. Liu, S. S. Hong, K. J. Koski, S.-K. Mo, Z. Hussain, I. R. Fisher, Z.-X. Shen, and Y. Cui, *Nat. Nano.* **6**, 705 (2011).
- [41] Y. G. Yao, L. Kleinman, A. H. MacDonald, J. Sinova, T. Jungwirth, D.-S. Wang, E. Wang, and Q. Niu, *Phys. Rev. Lett.* **92**, 037204 (2004).
- [42] D. Xiao, M. C. Chang, and Q. Niu, *Rev. Mod. Phys.* **82**, 1959 (2010).
- [43] S. Qi, Z. Liu, M. Chang, R. Gao, Y. Han, and Z. Qiao, *Phys. Rev. B* **101**, 241407(R) (2020).